Journal of Membrane Science 728 (2025) 124125

Contents lists available at ScienceDirect

Journal of Membrane Science

journal homepage: www.elsevier.com/locate/memsci

Nonsolvent-induced phase separation polyimide/polymeric ionic liquid separators for high-performance and safe lithium metal-based batteries

Yi-Hsiang Lin [a], Wei-Ming Huang [a], Jing-Yu Li [a], Mohamed Gamal Mohamed [a], Chi-Yung Tseng [b], Jian-Ming Chiu [b], Bing-Joe Hwang [b,c], Shiao-Wei Kuo [a], Yun-Sheng Ye [a,c,*]

[a] Department of Materials and Optoelectronic Science, Center of Crystal Research, National Sun Yat-Sen University, Kaohsiung, 80424, Taiwan
[b] Department of Chemical Engineering, National Taiwan University of Science and Technology, Taipei, 106335, Taiwan
[c] The Ministry of Education of Taiwan (the Sustainable Electrochemical Energy Development Center (SEED Center) from the Featured Areas Research Center Program, National Taiwan University of Science and Technology, Taipei, 106335, Taiwan

ARTICLE INFO

Keywords:
Polyimide thermotolerant separator
Nonsolvent-induced phase separation lithium metal-battery

ABSTRACT

Lithium-ion battery separator safety has grown significantly in recent years, and preventing or minimizing thermal runaway in Li-ion batteries, especially during rapid charging and discharging, is a crucial problem. Therefore, there is a pressing need to develop high-safety thermotolerant separators that can guarantee high ion transport while also enabling homogeneous Li^+ fluxes for the inhibition of Li dendritic growth. The nonsolvent-induced phase separation (NIPS) technique is used here to create a novel kind of polyimide (PI)/polymeric ionic liquid (PIL) separator that can be used as a thermotolerant separator alternative to commercial polyolefin-based separators. Without encountering a problem with other types of thermotolerant separators, whether they have nanopores or micropores, the fabricated PI/PIL separator with homogenous and nanosized pores exhibits high electrolyte adsorption/retention, ionic conductivity, mobility, and electrochemical properties in addition to typical high mechanical and thermal properties. Moreover, the PI/PIL separator displays excellent resistance for dendrite growth, and when integrated into the NCM811/Li cell demonstrates excellent cycling stability and rate performance. This work offers a significant method for creating a thermotolerant separator that addresses the issues of Li metal batteries, such as the absence of a high-performance and high-safety separator.

1. Introduction

The design criteria for the next generation of energy storage systems are high energy and power densities, high-rate capability and long-cycle reliability [1]. Nonetheless, regardless of the complexity of the features, battery safety remains an essential concern that cannot be neglected for any high-performance lithium metal battery (LMB) [2,3]. The separator, which physically isolates the cathode from the anode, is a vital component of a battery that enhances safety by inhibiting the conversion of stored chemical energy into heat [4]. On the other hand, the separator serves as a crucial medium for sustaining the liquid electrolyte and facilitating lithium ion transfer, which determines the interfacial resistance and performance of the resultant batteries [5]. However, the separator typically fails due to internal short circuits (ISC) [6] resulting from various conditions, including (i) uncontrollable thermal environments, (ii) unexpected collisions and extrusions, and (iii) unfavourable lithium dendrite formation. Given these conditions, the creation of separators with exceptional overall performance is a crucial yet challenging task for advancing high-performance energy storage devices.

Among the various separators developed to date, porous polyolefin-based separators, specifically polyethylene (PE)-, polypropylene (PP)-, and polytetrafluoroethylene (PTFE)-based separators, have emerged as the most prevalent for commercial Li-ion batteries over the years due to their advantageous characteristics, including cost-effectiveness, robust mechanical strength, optimal pore structure, electrochemical stability, and thermal shutdown capabilities [7–9]. However, several critical issues must be addressed, including nonpolarity, insufficient wettability and porosity (40–45 %), and low melting points (PP: 165 °C, PE: 135 °C), which further impede its application in batteries [10]. The first two factors generally cause inadequate compatibility between the separator and electrodes, obstructing ion migration and resulting in uneven lithium stripping and plating, which consequently leads to

* Corresponding author. Department of Materials and Optoelectronic Science, Center of Crystal Research, National Sun Yat-Sen University, Kaohsiung, 80424, Taiwan.
E-mail address: ysye@mail.nsysu.edu.tw (Y.-S. Ye).

https://doi.org/10.1016/j.memsci.2025.124125
Received 7 March 2025; Received in revised form 11 April 2025; Accepted 18 April 2025
Available online 19 April 2025

unsatisfactory cycling and rate performances [11]. The final factor is the most critical and the principal cause of separator failure and related safety hazards, including high-temperature fires and explosions. Decorating inorganic composites onto their surface is regarded as a promising strategy to not only mitigate these drawbacks but also to introduce new functionalities [12,13]. However, the intrinsic polyolefin matrix cannot maintain its structural integrity at elevated temperatures. The advancement of innovative polymer-based separators for LMB is sufficiently addressed; however, it continues to pose challenges, with only a limited number being employed for LMBs [14].

Thermotolerant separators, including ceramic, polybutylene terephthalate (PBT), polyether imide (PEI), and polyimide (PI), are recognized for their superior thermal properties and are considered advanced separators for enhancing the safety of LMBs [15,16]. A variety of preparation methods for thermotolerant separators include electrospinning, sacrificial templating, and phase inversion/separation [17–20]. The phase inversion method, which entails dissolving the polymer in a suitable solvent and subsequently converting it to create porous structures through solvent exchange with a poor solvent, has been considered an alternative technique for fabricating porous separators utilized in LMBs [15,18]. To date, thermotolerant porous separators, such as sponge-like porous PEI [21,22], sponge-like porous PBI [23], pPAN (poly (vinyl alcohol)-modified polyacrylonitrile) [24], and porous PI separators [25], have been fabricated using the nonsolvent-induced phase separation (NIPS) method, demonstrating significant thermal stability. However, the parameters of the NIPS method are challenging to regulate precisely, resulting in a discontinuous pore structure, a broad pore-size distribution, and insufficient porosity, which impede ion transport and induce inhomogeneous ion distribution during the operation of LMBs. A high porosity will not only result in poor electrolyte retention and dendrite formation but also compromise the mechanical integrity of the separator, thereby increasing the chances of punctures. Therefore, the development of highly porous separators with a uniform pore size distribution and nanopore dimensions via an effective NIPS method is essential for achieving high-performance and safe separators in LMB.

In recent years, polymeric ionic liquids (PILs) have emerged as potential materials for improved battery systems owing to their inherent ionic conductivity, electrochemical stability, and adjustable structural characteristics. In contrast to conventional polymer matrices, PILs integrate ionic moieties directly into their polymer backbones, facilitating effective ion transport while preserving mechanical integrity. Several studies have demonstrated that PILs can enhance Li-ion transference number, suppress dendrite formation, and improve interface compatibility with Li metal anodes [26,27]. These advantages make PILs attractive components in solid and gel polymer electrolytes. However, their integration into porous structural frameworks for separator design remains relatively underexplored. This study presents the fabrication of nanoporous polyimide membranes using the NIPS method, which were subsequently integrated with PIL to serve as thermotolerant separators for LMBs for the first time. As shown in Scheme 1, a soluble organic PI has been synthesized and employed as a polymer matrix to promote phase separation in an aqueous non-solvent. The amide comprising N, N'-(2,2′-bis(trifluoromethyl)-[1,1′-biphenyl]-4,4′-diyl) bis(4-aminobenz amide) (AB-TFMB) enhances stability and augments electrolyte affinity, facilitating the robust formation of the PI framework in the resultant membrane. The produced PI membrane possesses a relatively thin thickness of less than 7 μm and features nanopore structures, facilitating uniform ion migration over short transport distances. Furthermore, the infiltrated PIL can improve membrane stability and electrolyte retention, thereby reducing ion migration resistance and facilitating rapid and stable charging and discharging performance of the battery. This research facilitates the advancement of thermotolerant separators for LMBs and provides a novel approach for the suppression of Li dendrites.

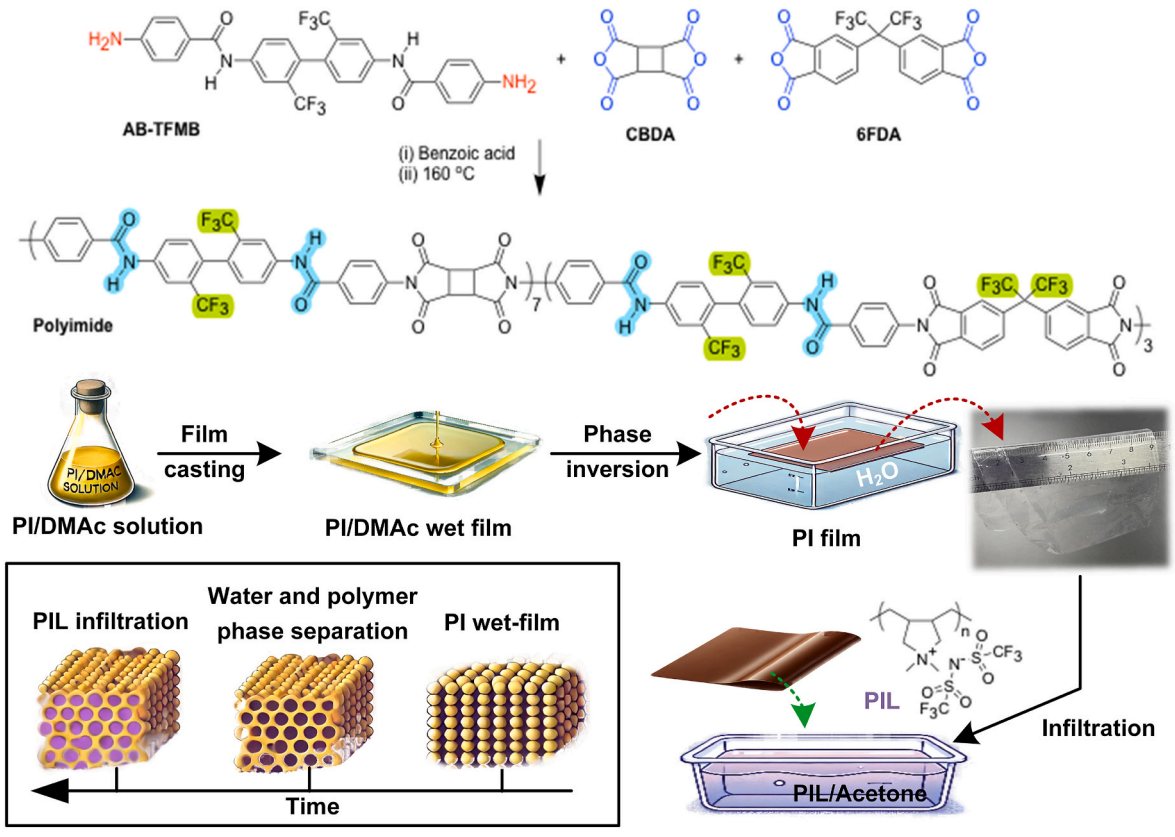

Scheme 1. Schematic illustration of PI/PIL separator fabrication.

2. Experimental section

Materials. 2,2′-bis(trifluoromethyl)-4,4′-bis [4-(4-amino-benzamide)] biphenyl (AB-TFMB), poly (vinylidene fluoride) (PVDF), 4,4'-(hexafluoroisopropylidene)diphthalic anhydride (6FDA), 1,2,3,4-cyclobutanetetracarboxylic dianhydride (CBDA), and benzic acid purchased from Leyan Technologies. dimethylacetamide (DMAc), Acetone, dimethylformamide (DMF), N-methyl-2-pyrrolidone (NMP), ethylene carbonate (EC), dimethyl carbonate (DMC), dimethyl ether (DME), 1,3-Dioxolane (DOL), lithium nitrate ($LiNO_3$) from Echo Chemcial Co Ltd. Commercial Celgard (2325) trilayer separators were provided by Dongguan Saidiou Electronic Technology Co. $LiNi_{0.8}Co_{0.1}Mn_{0.1}O_2$, NCM811 was purchased from SHANSHAN Corporation. Benchmarking electrodes were constructed from Super P® carbon, obtained from Alfa Aesar (UK). PIL containing TFSI anions was obtained via ion exchange from a poly (diallyldimethylammonium chloride) (PDDA) solution (20 wt% in H_2O) using lithium bis(trifluoromethanesulfonyl)imide (LiTFSI). PDDA solution was purchased from Macklin Biochemical Co., Ltd. (Shanghai, China). LiTFSI was purchased from TCI Chemicals and dried under vacuum at 180 °C for 24 h to remove moisture.

Fabrication of PI/PIL separator. The PI separator was synthesized via NIPS. Initially, DMAc was utilized as a solvent to formulate a 5 wt% PI solution at 60 °C for 12 h. The resultant PI solution was applied onto a glass plate using a blade and subsequently immersed in a nonsolvent coagulation bath (deionized water, DI) at 60 °C for 10 min to enhance the polymer's solidification. The prepared PI thin film was subsequently transferred into EtOH via the solvent exchange method. The wet PI thin film was subsequently infiltrated with a 3 wt% PIL/acetone solution and then dried at 60 °C to yield a PI/PIL film.

Preparation of NCM811 and sulfur cathodes. NCM811, super P, and PVDF were combined in a weight ratio of 93:3:4 in anhydrous NMP solution by MSK-PCE-V2150 and uniformly applied to the Al foil using a baler. The naturally dried electrodes underwent vacuum drying at 70 °C for 12 h. The electrode lugs were ultimately stamped into discs with a diameter of 12 mm and a face mass loading of cathode material of approximately 1.8 mg cm^{-2}. The fabricated S-cathode had a sulfur loading of 1.5 mg cm^{-2}, and the sulfur cathode was made using a similar method.

Assembly of the NCM811/Li and Li–S cells. [28] Inside a glovebox filled with Ar (MBraun, O_2, and $H_2O \leq 0.1$ ppm), NCM811/Li cells were assembled. All measurements were carried out at 40 °C with an initial equilibration time of 1 h allowed for electrode wetting and temperature uniformity. PP and PI/PIL separators, soaked in 50 μL of electrolyte (1 M $LiPF_6$ in EC: DMC = 1:1 v/v). The cells were cycled at voltages ranging from 3.0 to 4.35 V vs Li^+/Li under varied current rates from 0.2 C to 4 C. For Li–S batteries, the electrolyte (DOL: DME = 1:1 v/v containing 1 wt % $LiNO_3$)-to-separator (E/S) ratio for Li–S cell assembly is 20 μL mg^{-1}.

Material characterization. The separators were characterized by scanning electron microscopy (SEM) (FEI Nova NanoSEM450). Transmission electron microscopy (TEM, thermo Fisher Scientific, Talos F200X). Thermogravimetric analysis (TGA, Q50) from room temperature to 800 °C at a heating rate of 10 °C min^{-1} under N_2 atmosphere.

Electrochemical measurements. Electrochemical impedance spectroscopy (EIS), linear sweep voltammetry (LSV), and constant-current charge-discharge curves were conducted utilizing a Land CT3002A test system.

The porosity (φ) of the separators was assessed using the n-butanol immersion technique. The desiccated samples were immersed in n-butanol for 24 h at ambient temperature, and the porosity was determined using the subsequent equation:

$$\boldsymbol{\varphi} = (\boldsymbol{M_b} / \boldsymbol{\rho_b}) / (\boldsymbol{M_b} / \boldsymbol{\rho_b} + \boldsymbol{M_d} / \boldsymbol{\rho_d}) \times \mathbf{100\%} \quad \text{(Eq 1)}$$

The weights of the samples before and after immersion in n-butanol are denoted as M_d and M_b, while ρ_b and ρ_d represent the densities of n-butanol and the polymer, respectively.

The electrolyte uptake (*EU*) and electrolyte retention (*ER*) for the separators were estimated by the following equation:

$$\boldsymbol{EU}(\%) = (\boldsymbol{W_s} - \boldsymbol{W_d}) / \boldsymbol{W_d} \times \mathbf{100\%} \quad \text{(Eq 2)}$$

$$\boldsymbol{ER}(\%) = (\boldsymbol{W_t} - \boldsymbol{W_d}) / \boldsymbol{W_d} \times \mathbf{100\%} \quad \text{(Eq 3)}$$

where W_d is the separator's initial mass and W_s is its mass following a 1 h immersion in the electrolyte. W_t is the separator's mass following a predetermined drying time.

The ionic conductivity of the separator was determined by evaluating the electrochemical impedance of an SS/separator/SS symmetric cell utilizing an AutoLab electrochemical workstation, employing the subsequent equation:

$$\boldsymbol{\sigma} = \boldsymbol{d}/\boldsymbol{R}\cdot\boldsymbol{S} \quad \text{(Eq 4)}$$

Where *s*, *d*, *S*, and *R* represent the ionic conductivity, thickness of the separator, SS current collector (2.01 cm^2), and bulk resistance.

The separators swollen in 1 M LiPF6 EC/DMC electrolyte were included into symmetric Li metal cells to assess the Li^+ transference number (t_{Li^+}) using the Bruce-Vincent method [29].

$$\boldsymbol{t_{Li^+}} = \boldsymbol{I_{SS}}(\Delta\boldsymbol{V} - \boldsymbol{I_0}\boldsymbol{R_0}) / \boldsymbol{I_0}(\Delta\boldsymbol{V} - \boldsymbol{I_{SS}}\boldsymbol{R_{SS}}) \quad \text{(Eq 5)}$$

Where ΔV denotes the potential applied across the cell, R_0 and R_{SS} represent the initial and steady-state resistances of the passivating layers as determined by impedance spectroscopy, and I_0 and I_{SS} signify the initial and steady-state currents during polarization, respectively.

Li ion behaviours in an NMC811/Li cell with separators were investigated using a GITT. It is commonly known that Fick's 2nd Law of diffusion, which can be expressed as the following equation, can be used to calculate the Li ion diffusion coefficient (D_{Li^+}) of Li ions [30,31]:

$$\boldsymbol{D_{Li^+}} = \mathbf{4} / \boldsymbol{\pi\tau}\ \left(\boldsymbol{n_m}^2\ \boldsymbol{V_m^2}\right) / \boldsymbol{S}\ \left(\boldsymbol{\Delta E_S^2}\right) / \left(\boldsymbol{\Delta E_T^2}\right) \quad \text{(Eq 6)}$$

Where ΔE_s is the evolution of the steady-state voltage, and ΔE_t represents the voltage variation during the constant-current pulse, including the IR drop. τ is the current pulse (s), nm is the number of moles (mol), V_m is the molar volume of the active material (cm^3 mol^{-1}), and S is the electrode/electrolyte contact area (cm^2).

3. Results and discussion

Fabrication and formation mechanism of the PI/PIL separators. The fabrication of porous PI separators was achieved through the NIPS synthesis strategy, as illustrated in Scheme 1. The synthetic composite separators of PI/PIL were produced utilizing PI and PIL as basic building blocks. The former serves as the substrate for framework construction in separators due to its thermal stability, mechanical robustness, and exceptional chemical and electrochemical stability in LMBs, whereas the latter functions as a stabilizer to enhance the pore structure and retain the electrolyte within the prepared separator. The non-conjugated molecular structure of CBDA and the fluorine-rich molecules of 6FDA imparted exceptional solubility in the reaction medium, thereby enabling the effective utilization of NIPS for the direct fabrication of PI membranes. The synthesized PI exhibited solubility in polar aprotic solvents, including N,N-dimethylformamide (DMF), DMAc, and 1-methyl-2-pyrrolidone (NMP). The excellent solubility of PI in organic solvents facilitated the confirmation of the structure through ^{1}H NMR measurements, as depicted in Fig. 1. The results indicated that the distinctive absorptions of hydrogen protons in the amide (–CONH–) group (peak c) and in the aromatic rings (peaks a, b, d, e, and f) were clearly identified. Moreover, the absorptions of the cyclobutane protons appeared upfield in the spectra owing to the electron-donating characteristics of the alicyclic rings. The ratio of the AB-TFMB-CBDA segment to AB-TFMB-6FDA, based on their characteristic peak area, is 6.8 to 3.2, agreeing with our expectations from the experimental design. The ^{13}C NMR results indicate distinct characteristic peaks (peaks 13, 16, and 5)

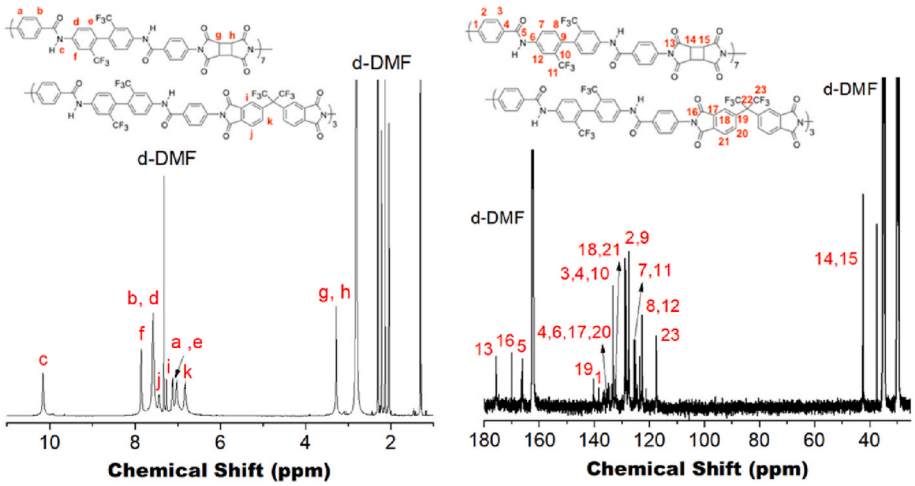

Fig. 1. ^{1}H NMR and ^{13}C NMR spectra of PI.

downfield in the spectra, corresponding to the C═O groups from the imide ring and amide functional group. Likewise, the cyclobutane carbons manifested upfield in the spectra. The results align with the structural characteristics of the synthesized PI.

The PI/DMAc solutions were cast into solid-state films and subsequently immersed in deionized water coagulating baths, which served as a non-solvent. Upon exposure of the cast PI sol-state liquid films to a water bath, the rapid exchange rate between DMAc and water resulted in the formation of relatively dense films with nanopores [32,33]. The robust hydrogen bonding established by the amide groups of the AB-TFMB repeat unit diminishes the phase separation rate, leading to the formation of uniformly distributed pores within the resultant PI separator. The prepared PI film, without prior drying, conducted solvent exchange with EtOH and was subsequently immersed in a PIL/acetone solution to promote the infiltration of PIL into its pores. Infiltration of PIL into PI film can stabilize the pore size structure of PI, attributed to the IL groups in PIL, while the amide groups in PI can establish a stable network structure around the pores through ionic bonds as the binding forces.

Characterization of the PI/PIL separator. The morphologies of PI/PIL separators, illustrated in Fig. 2a, demonstrate a thickness of less than 7 μm, characterized by a dense and smooth structure, lacking detectable micro- and nano-sized pores. This study further examined the separators absent of PIL infiltration to analyze the dimensions and distribution of pores in the PI/PIL more efficiently. The resulting film demonstrates comparable thickness (Fig. 2b), and its magnified area is presented in Fig. 2c. The cross-sectional image distinctly reveals that the significantly darker areas, attributed to the pores, measure less than 10 nm and display a consistent distribution throughout the membrane, resulting in numerous pores that enable broad paths for ion movement. The HRTEM image (Fig. 2d) further depicted the highly porous structures with pore sizes less than 5 nm, corresponding to the relatively lighter regions and significant porosity throughout the entire PI film. The porosity test results indicate that the PI film exhibits a high porosity of 60.1 %.

The thermal stability of the separator significantly influences the safety of lithium metal batteries, particularly during rapid charging and discharging cycles [34]. Fig. 3a illustrates that TGA experiments indicate PP begins to decompose at approximately 220 °C, with total weight

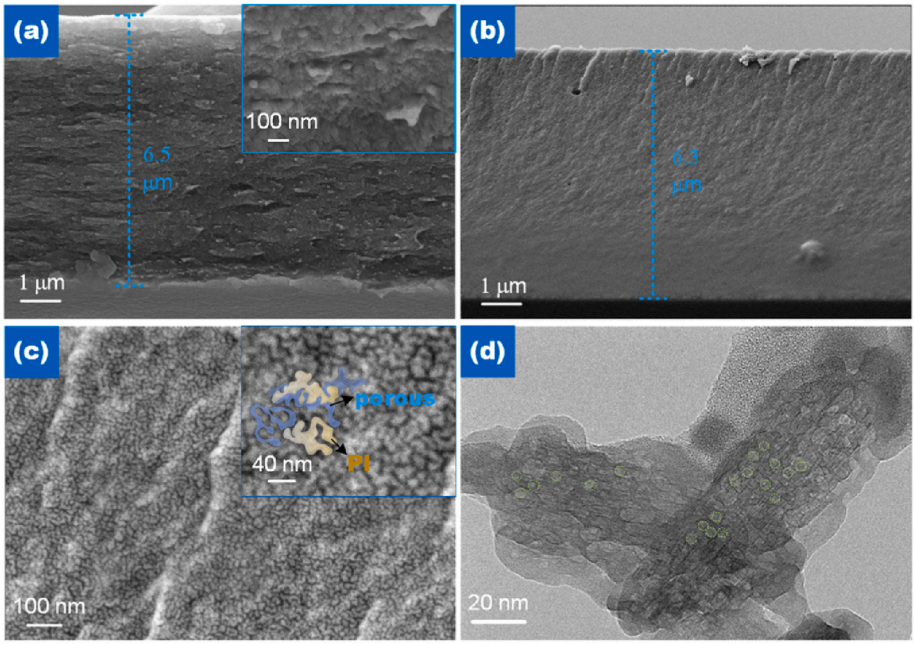

Fig. 2. Cross-sectional SEM images of (a) PI/PIL and (b, c) PI without PIL infiltration. TEM image of the porous PI separator.

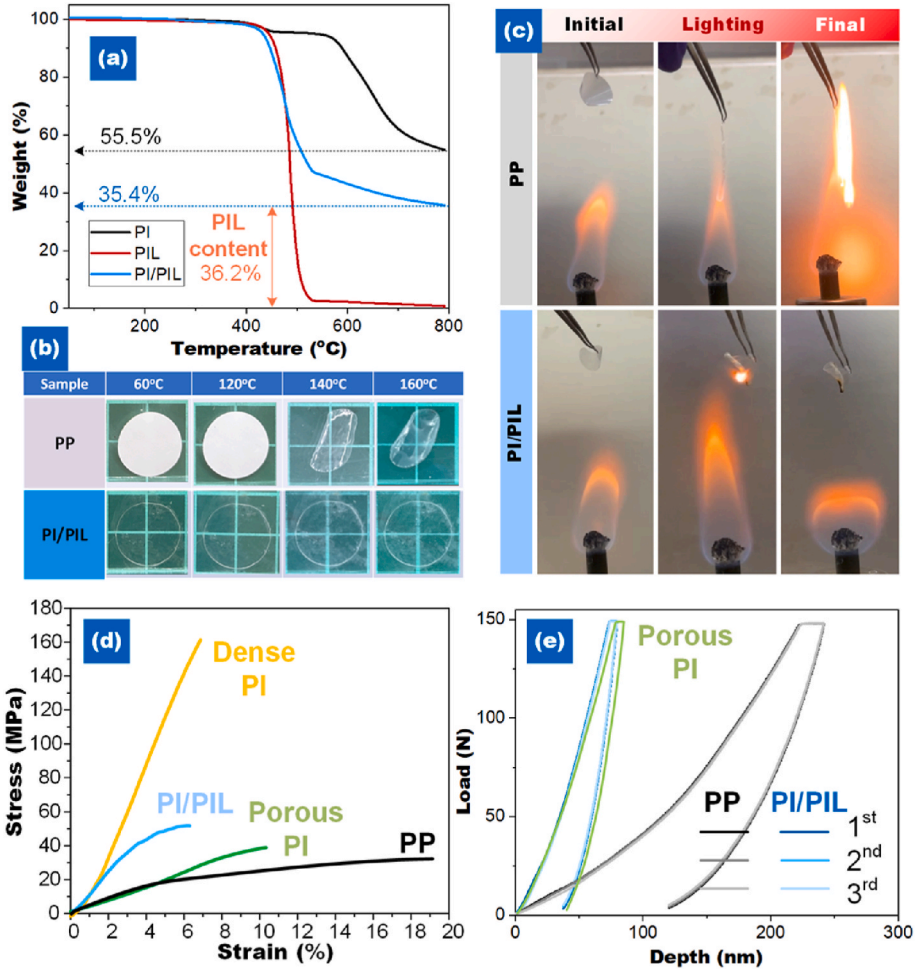

Fig. 3. (a) TGA curves of PI, PIL, and PI/PIL. (b) the images of PP and PI/PIL separators after heat treatment at different temperatures for 5 min. (c) Time dependence of burning liquid electrolyte in the PP and PI/PIL. (d) Stress-strain and (e) load vs. displacement curves for the PP, porous PI, and PI/PIL.

loss occurring at 450 °C, whereas the fabricated PI/PIL separator exhibits no significant weight loss at 420 °C. The TGA results indicate that the PIL content in the PI/PIL separators is 55.5 % based on the yield of pristine PI and PIL. As illustrated in Fig. 3b, no significant shrinkage of the PI/PIL separator was detected when the temperature increased from 60 °C to 160 °C, whereas the PP separator completely melted at 140 °C. Furthermore, the shrinkage ratio of the PI/PIL separator remains nearly constant, demonstrating its exceptional thermal stability. The flammability of the liquid electrolyte in the separators was assessed through combustion testing. Fig. 3c presents the time dependence of the burning liquid electrolyte/separator. When the separators are placed above the flame, the PI/PIL separator exhibits no combustion (>10s), in contrast to the PP, which ignites vigorously within 2s. The findings indicate that the PI/PIL separator exhibits superior mechanical robustness compared to the commercial PP separator at elevated temperatures, thereby mitigating the risk of short-circuits and associated safety concerns.

The mechanical properties of PP, dense PI, porous PI, and PI/PIL separators were assessed using tensile strength testing, with the resultant stress-strain curves illustrated in Fig. 3d. The pristine PI without a porous structure displays a tensile strength of 161.2 MPa, with a strain value of 6.9 %. Despite the introduction of pores into PI using the NIPS method, resulting in a tensile strength of 39.2 MPa, this strength still exceeds that of the PP separator, which is 30.3 MPa. Furthermore, following the infiltration of PIL, the tensile strength rises to 51.1 MPa, indicating that PIL may act as a reinforcing phase for the porous PI structure. The constructed PI/PIL separator exhibits remarkable mechanical strength at an ultra-thin thickness of under 7 μm, exceeding the performance of the majority of reported ceramic-based separators [35, 36]. Furthermore, nanoindentation is utilized to assess the resistance properties against Li dendrite formation. Fig. 3e illustrates the load versus displacement curves for the PP, porous PI, and PI/PIL separators, demonstrating hysteresis and creep, characteristics of the visco-elasto-plastic behavior of polymers. The findings indicate that the PP exhibits an indenter displacement of 243 nm within the bimodal distribution. It is noteworthy that both porous PI and PI/PIL exhibit a significantly smaller indenter displacement of ~80 nm, which is merely one-third of that of the PP separator. Furthermore, the PI/PIL separator exhibits a superior Young's modulus of 7.5 × 10^5 GPa compared to the PP separator of 203.5 GPa. The aforementioned results demonstrate that the PI/PIL separator exhibits significant resistance to the growth of Li dendrites [37].

Electrochemical properties and battery performances of the PI/PIL separator. Electrolyte uptake (*EU*), electrolyte retention (*ER*), electrolyte wettability are critical characteristics of separators that influence electrolyte penetration and ion-transport resistance. Fig. 4a demonstrates that both PI-based separators exhibit enhanced affinity for the liquid electrolyte due to the presence of polar amide groups and increased surface energy. The porous PI demonstrates a very high *EU* of 370 % attributable to its highly porous architecture. After infiltration of PIL, the *EU* of the resulting PI/PIL slightly decreased to 267 %; however, this value still remains significantly higher than that of the PP separator (119 %), indicating its excellent electrolyte absorption capability. However, for *ER*, the presence of PIL further enhances the ability of porous PI to retain the electrolyte, which also implies that the PI/PIL

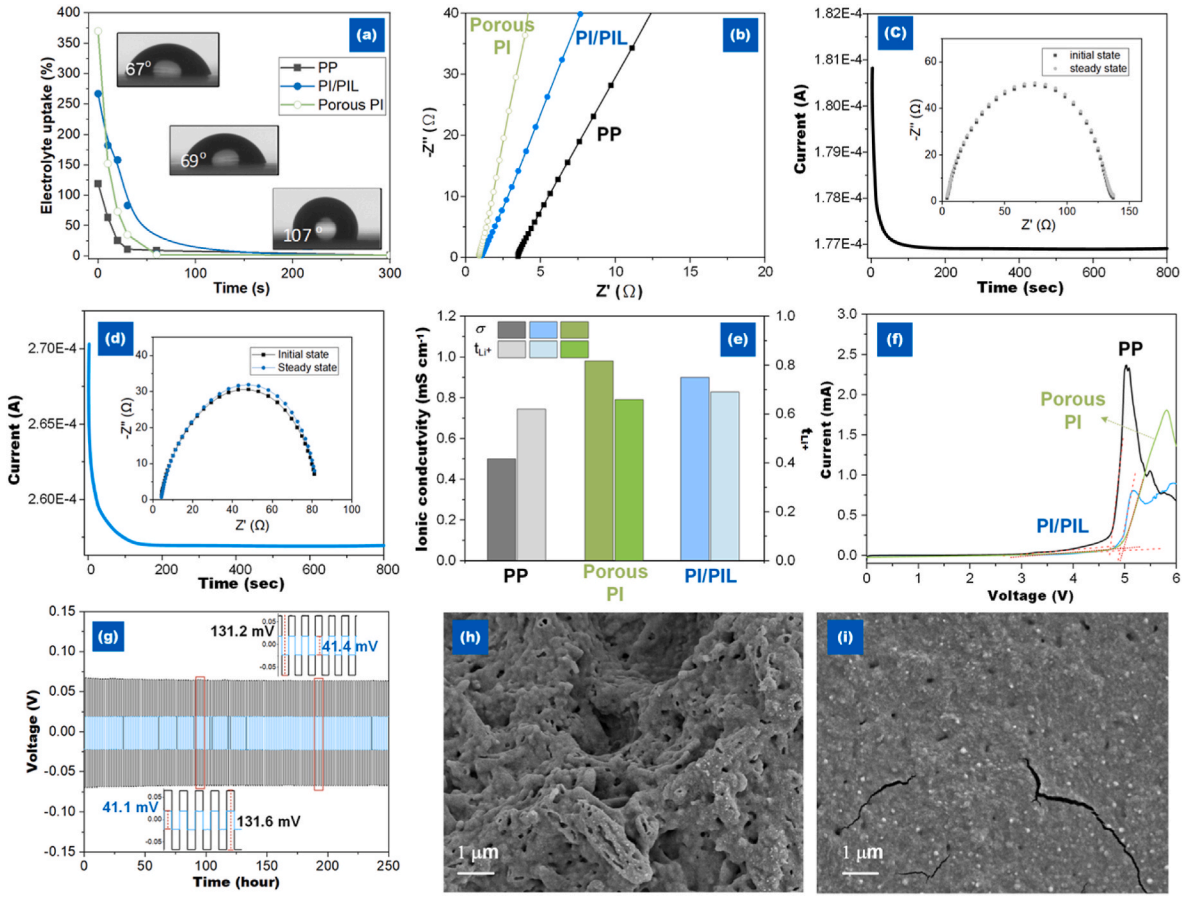

Fig. 4. (a) Electrolyte uptake and contact angle of PP, porous PI, and PI/PIL separators. (b) EIS spectra of SS/separators/SS batteries at room temperature. Impedance response of (c) PP and (d) PI/PIL prior to and subsequent to potentiostatic hold, along with current response during the potentiostatic hold. (e) Ionic conductivity and t_{Li^+} of PP, porous PI, and PI/PIL separators. (f) LSV curves of PP, porous PI, and PI/PIL separators. (g) Cycling performance of the Li/separator/Li symmetric cells. SEM images of Li metals disassembled from symmetric cells with (h) PP and (i) PI/PIL separators.

separator is more favorable for interfacial stability and long-term battery operation. As presented in the electrochemical impedance spectra (EIS) (Fig. 4b), the specific values of internal resistance for the PP, porous PI, and PI/PIL are 3.4, 1.0, and 1.1 Ω, respectively. The ionic conductivity (σ) of the PI/PIL separator (0.9 mS cm^{-1}) surpasses that of the PP separator (0.5 mS cm^{-1}), primarily owing to the enhanced electrolyte absorption of PI/PIL and the structural characteristics of infiltrated PIL that promote efficient Li^+ transport, thereby enabling rapid Li-ion movement across the separator. Fig. 4c and d illustrate the impedance before and after polarization and the current profile during the polarization with PP and PI/PIL separators swollen in 1 M $LiPF_6$ EC/DMC, respectively. The estimated t_{Li^+} values of PP and PI/PIL are 0.62 and 0.69, respectively, based on measurements on three different coin cells. The elevated t_{Li^+} value of PI/PIL signifies that Li^+ ions are preferentially transported compared to anions within the cationic PIL medium. These characteristics of PIL become more evident when compared with porous PI in Fig. 4e. Despite porous PI displaying a superior *EU*, the PI/PIL membrane still reveals a greater t_{Li^+}, which is beneficial for its improved performance in long-cycle and rate-capability evaluations.

The electrochemical stability window of the separator is crucial for sustaining the charge-discharge voltage during battery operation, which can be assessed through linear sweep voltammetry (LSV) experiments. Fig. 4f illustrates that the current in both PI-based separators, with or without PIL infiltration, maintains a stable voltage exceeding 4.9 V, attributable to the stable PI structure, corroborating prior research findings [38]. When compared with the PP separator (4.7 V), the PI/PIL separator exhibits superior voltage stability. The reversibility of Li electroplating and stripping for separators was assessed using Li/Li symmetric cells. Fig. 4g illustrates that the symmetric cell with PP and PI/PIL demonstrated a consistent electrochemical signal for Li plating/stripping at 0.5 mA cm^{-2}. The cycle life of the Li-symmetric cell with PI/PIL is significantly longer and exhibits a lower charge-discharge polarization voltage gap (~41 mV) compared to that with PP (~131 mV) after 200 h. This phenomenon may be attributed to diminished concentration polarization resulting from pore uniformity; areas with small pore distribution exhibit lower ion concentration and a more uniform ion migration rate, facilitating more uniform dendrite growth, which subsequently reduces short-circuiting after reaching a certain threshold [39]. The reduced polarization in the PI/PIL cell was further supported by the cross-sectional SEM images of the cycled Li metal (Fig. 4h and i). Following 200 h of cycling, a dense and uniform coating without apparent dendrites was observed on the surface of the Li foil from the PI/PIL symmetric cell (Fig. 4i). In contrast, the excessive Li dendrites are evident on the Li metal surface (Fig. 4h), which will continuously consume the electrolyte and enlarge the thickness of the SEI layer, leading to progressively greater polarization. The enhanced cycling performance and consistent plating/stripping potential indicate that the developed PI/PIL is superior for establishing a stable SEI layer on the Li electrode surface. These results demonstrate that the PI/PIL separator effectively stabilizes the Li plating/stripping behavior during long-term cycling. The superior performance can be attributed to the regulation of Li^+ flux and suppression of dendritic growth, which originate from the uniform ionic transport pathways, high t_{Li^+}, and improved electrolyte affinity of the PIL component. Together, these factors contribute to more homogeneous Li deposition and enhanced interfacial stability.

The impact of PP and PI/PIL separators on the cycling and rate performance of NCM811/Li cells is further examined within the voltage range of 3.0–4.35 V at current densities ranging from 0.2 to 4.0 C. The results show that both cells exhibit comparable capacities of 164.4 and 166.2 mA h g^{-1} at the 10th cycle for the PP and PI/PIL assembled cells, respectively (Fig. 5c). Nevertheless, after 100 cycles the PP-assembled cell exhibited a capacity decline to 116.6 mA h g^{-1}, resulting in a capacity retention of 70.9 %, whereas the PI/PIL maintained a superior capacity of 146.9 mA h g^{-1} with a capacity retention of 88.4 %. After 200 cycles, the PI/PIL assembled cell demonstrates a distinct plateau and provides a significantly higher capacity of 136.3 mA h g^{-1}, with a capacity retention of 82.0 %, in contrast to the PP assembled cell, which has a capacity of 74.1 mA h g^{-1} and a capacity retention of 45.1 % (Fig. 5a and b). Furthermore, the capacity retention of the PI/PIL assembled cell can be maintained at 57.0 % after 300 cycles even without the addition of the electrolyte additive vinylene carbonate (VC), nearly double that of the PP assembled cell (29.4 %). The NCM811/Li cell utilizing a PI/PIL separator exhibits superior cyclic stability compared to cells employing a PP separator.

The electrochemical impedance spectroscopy (EIS) analysis of PP and PI/PIL assembled cells before/after long-term cycling is conducted to elucidate the resistance associated with ion and electron transfer within the battery. All the EIS spectra consist of a quasi-semicircle in the high-to medium-frequency range and a linear segment in the low-frequency range. The high-medium frequency region of the quasi-semicircle denotes the charge transfer resistance (R_{ct}) associated with electron/ion migration at the electrode/electrolyte interface, while the low-frequency region of the straight line, known as Warburg diffusion, relates to the diffusion of Li^+ within the bulk of electrode materials [40, 41]. Clearly, as illustrated in Fig. 5d and e, the PI/PIL assembled cell exhibits reduced interfacial resistance in comparison to the cell with PP, signifying that the PI/PIL demonstrates superior interfacial contact with the electrode. Moreover, the PI/PIL assembled cell exhibits a reduced variation in R_{ct} ($\Delta R_{ct} = 200.4\ \Omega$) after 300 cycles in contrast to the PP assembled cell ($\Delta R_{ct} = 290.9\ \Omega$), due to several advantages, including (i) enhanced electrolyte affinity and absorption, (ii) elevated ionic conductivity, (iii) superior electrolyte retention, and (iv) improved interfacial stability, which collectively alleviate the adverse effects caused by the expanded interface. The long-term cycling of NCM811/Li cells was conducted, and the resultant separator and Li electrode were extracted from the cycled cells. As depicted in Fig. 5f and g, the Li metal obtained from the cycled PP-assembled cell exhibited a markedly rough surface with protruding, moss-like Li dendrites compared to the PI/PIL-assembled cell after cycling. The cycled PP exhibited considerable damage, characterized by a pronounced and extensive rough surface (Fig. 5h and i), whereas a smoother surface was noted in the cycle PI/PIL, attributed to the even ion flux and superior mechanical performance of the PI/PIL separator.

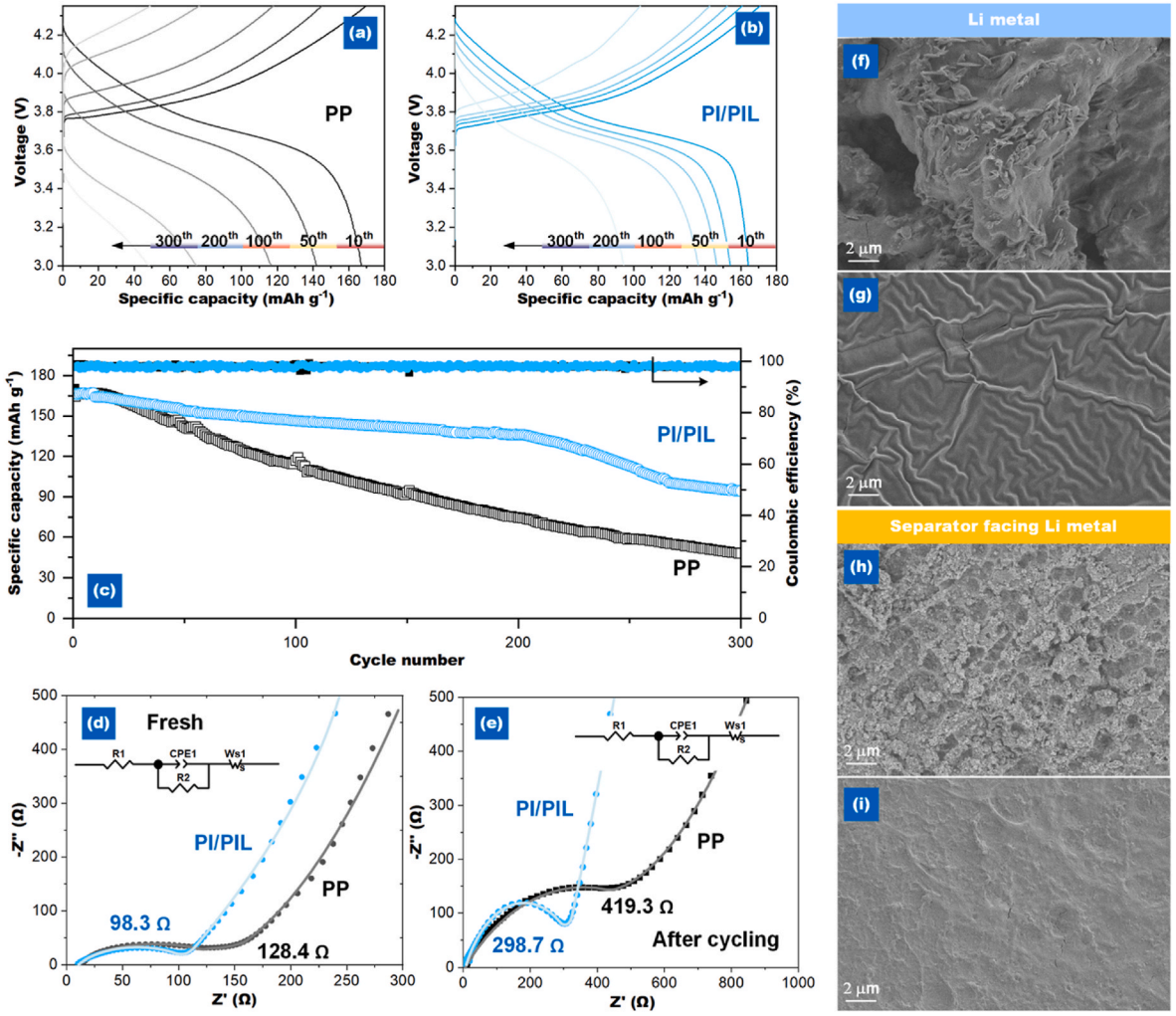

Fig. 5. Charge-discharge profiles of the NCM811/Li cells with (a) PP and (b) PI/PIL separators at 0.5 C. (c) cycling performance of the NCM811/Li cells with PP and PI/PIL. EIS of the (d) PP and (e) PI/PIL separators. SEM photos of the separator facing Li metal and Li metal obtained from cycled NCM811/Li cells with (f) (h) PP and (g) (i) PI/PIL separators.

Fig. 6a–c illustrate the charge-discharge profiles and rate performance of NCM811/Li cells utilizing PP and PI/PIL separators. Due to enhanced ion conductivity and favorable affinity with the liquid electrolyte, the PI/PIL assembled cell demonstrated reversible rate capabilities as the current density increased from 0.2 to 4 C, yielding discharge capacities of 170.5, 156.8, 136.9, 121.8, and 103.6 mA h g^{-1}. Fig. 6a and b illustrate voltage profiles exhibiting smooth platforms across a range of rates from 0.2 to 4 C. In contrast, the discharge capacities of the PP-assembled cell are merely 169.5, 144.7, 123.0, 86.8, and 56.3 mA h g^{-1}, accompanied by significant capacity degradation. Furthermore, at a current recovery of 0.2 C, the PI/PIL assembled cell continues to provide 155.6 mA h g^{-1}, demonstrating significantly greater stability compared to the PP assembled cell, which yields 111.9 mA h g^{-1}. The unsatisfactory rate performance in PP-assembled cells might result from the intrinsically large pore distribution, accompanied by a pronounced ion concentration polarization on both sides of the separator, particularly at elevated current densities.

The Galvanostatic Intermittent Titration Technique (GITT), based on Fick's law and quantifying the mobile ions at the electrolyte-electrode interface, was utilized to assess the redox reaction and proliferation kinetics in the PP and PI/PIL assembled cells. Fig. 6d and e illustrate the GITT results of PP and PI/PIL assembled cells, depicting the variations in current and voltage over time, associated with the calculated diffusion coefficient. Fig. 6d illustrates the GITT profiles of the cells, with the potential hysteresis noted during the relaxation phase corresponding to the excess potential of the polylithiation platform. The inset figure illustrates that the initial condition is in a state of equilibrium, characterized by a uniform concentration of mobile ions across the electrode [42]. Upon the application of a constant current pulse, a sudden voltage transition from E_1 to E_2 occurs due to the current flux manifesting as an IR drop. During the current duration ($\tau = 60$ min), the mobile ions are deintercalated from the host materials, resulting in a voltage change to E_3. After the constant current pulse, the voltage diminishes once more due to an IR drop. In the relaxation period (120 min), the electrode's composition attains homogeneity through Li^+ diffusion within the materials, resulting in the voltage stabilizing at a new equilibrium state, E_4. The results show that the PI/PIL assembled cell demonstrates a lower ΔV compared to the PP-assembled cell during the repeated charge-discharge process between operation and equilibrium. The chemical diffusion coefficients ($\boldsymbol{D}_{Li^+}$) can be calculated from different states of charge (SOCs) in the material through repeated galvanostatic titration during charging and discharging processes. Fig. 6e depicts the measured $\boldsymbol{D}_{Li^+}$ as a function of normalized time, revealing that the cell with PI/PIL displays increased values during both charging and discharging processes, signifying enhanced electrochemical reactions due to superior Li ion mobility within the PI/PIL separator.

To assess practical applications of NCM811/Li cells, we examined the impact of self-discharge caused by parasitic reactions [30,31]. Fig. 6f illustrates the open-circuit voltage (OCV) of the cell, recorded continuously over a period of 72 h. The PI/PIL assembled cell demonstrates

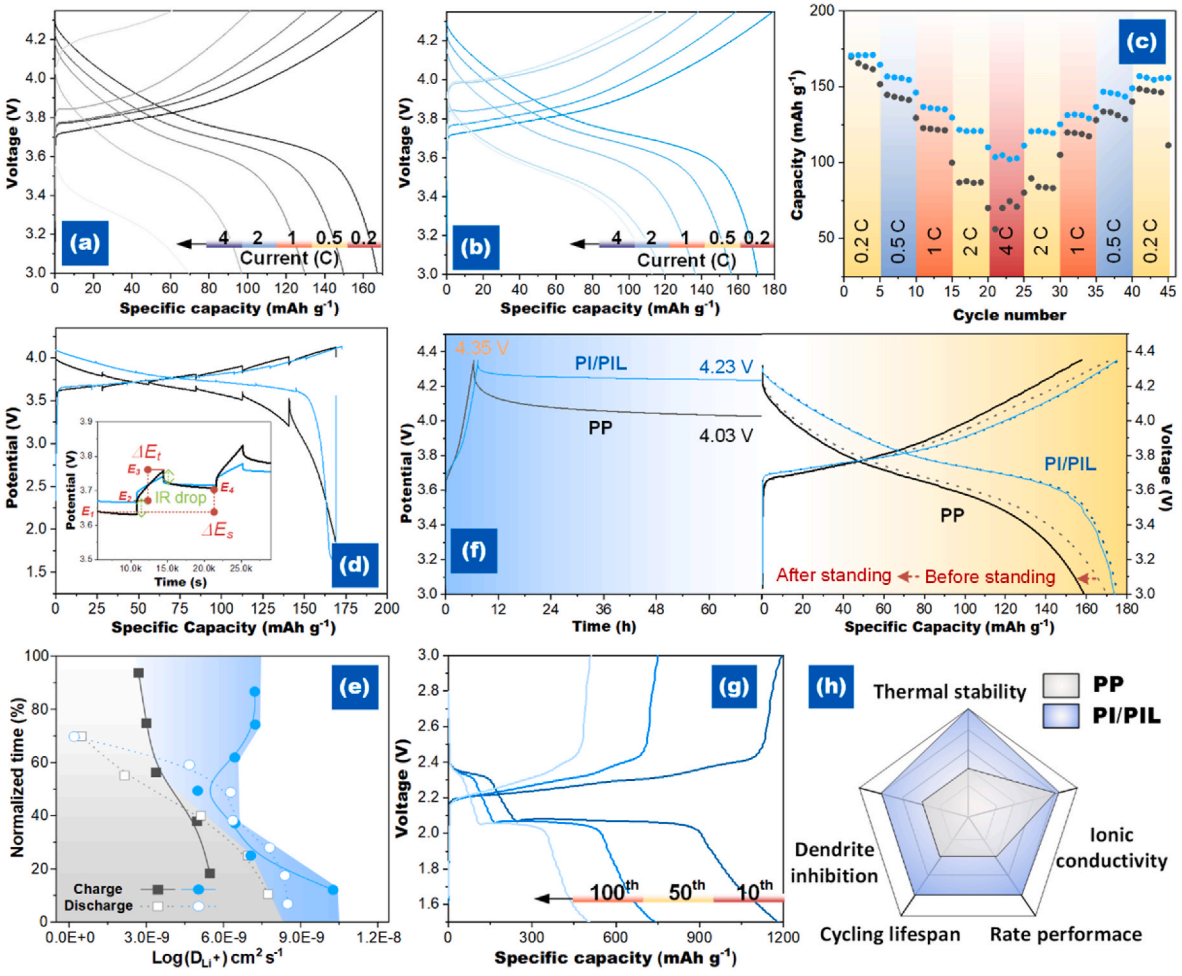

Fig. 6. Charge-discharge profiles of the NCM811/Li cells with (a) PP and (b) PI/PIL separators at various currents. (c) Rate performance of NCM811/Li cell with PP and PI/PIL. (d) GITT profiles and (e) calculated Li ion diffusion coefficient of NCM811/Li cell with PP and PI/PIL. (f) 5th cycled voltage-time profiles of NCM811/Li cell with PP and PI/PIL separators. (g) charge-discharge profile of Li–S cell with PI/PIL separator at 0.5 C. (h) Comparison of the comprehensive performance for PP and PI/PIL separators.

significantly enhanced stability in OCV, with a final voltage of 4.23 V, in contrast to the PP assembled cell's 4.03 V. Furthermore, the PI/PIL assembled cell demonstrated a capacity of approximately 169 mA h g^{-1}, which remained mostly unchanged. On the contrary, the PP-assembled cell demonstrated a notable decrease in capacity loss of 11 mA h g^{-1}. Li–S batteries also used the PI/PIL separator, and Fig. 6g displays the resulting galvanostatic discharge-charge profiles. The outcome confirms the high potential of PI/PIL separator as LMBs by demonstrating that Li–S cells with PI/PIL separators exhibit a high capacity of 1179.5 mA g h^{-1} at 0.5 C and maintain a satisfice capacity of 502.6 mA g h^{-1} after 100 cycles. Fig. 6h summarizes the property parameters of PP and PI/PIL separators. The PI/PIL separator demonstrates superior overall performance across all five dimensions, positioning it as a promising separator for LMBs and beyond.

4. Conclusions

In summary, we used the NIPS technique to develop nanoporous PI membranes with ultra-thin thickness, high porosity, and thermally stable properties. The PI/PIL separator that is produced with PIL's support has good ion conductivity, high ion mobility, and remarkable electrochemical performances. The following factors explain the superiority of the PI/PIL separator over PP: (i) the genuine deposition of Li metal on the electrode can be induced by the homogeneous and nanosized pores of PI; (ii) the amide containing PI and infiltrated PIL has a stronger affinity for the electrolyte than PP, which results in better wettability of the separator towards the electrolyte; (iii) high electrolyte uptake and wettability of PI/PIL contribute to high ion conductivity and mobility; (iv) the built PI skeleton PI and infiltrated PIL exhibits higher mechanical strength compared to PP. As a result, the NCM811/Li cell with PI/PIL separator exhibits superior rate performance, self-discharge resistance, and cycling stability than the PP-assembled cell. This work offers fresh concepts and techniques for PI/PIL separator manufacturing, which could aid in the development of high-performance and safety LMBs.

CRediT authorship contribution statement

Yi-Hsiang Lin: Software, Methodology, Conceptualization. **Wei-Ming Huang:** Formal analysis, Data curation. **Jing-Yu Li:** Formal analysis, Conceptualization. **Mohamed Gamal Mohamed:** Investigation, Formal analysis. **Chi-Yung Tseng:** Resources. **Jian-Ming Chiu:** Resources. **Bing-Joe Hwang:** Resources, Investigation. **Shiao-Wei Kuo:** Supervision, Resources. **Yun-Sheng Ye:** Writing – review & editing, Writing – original draft, Funding acquisition.

Declaration of competing interest

The authors declare the following financial interests/personal relationships which may be considered as potential competing interests: Yun-Sheng Ye reports financial support was provided by National Science and Technology Council. If there are other authors, they declare that they have no known competing financial interests or personal relationships that could have appeared to influence the work reported in this paper.

Acknowledgements

We acknowledge financial support from the National Science and Technology Council (NSTC) (112-2222-E-110-007-MY2) and analytical assistance from the Instrumentation Center at National Sun Yat-sen University.

Data availability

Data will be made available on request.

References

[1] S. Yuan, K. Ding, X. Zeng, D. Bin, Y. Zhang, P. Dong, Y. Wang, Advanced nonflammable organic electrolyte promises safer Li-Metal batteries: from solvation structure perspectives, Adv. Mater. 35 (13) (2023) 2206228, https://doi.org/10.1002/adma.202206228.
[2] B. Song, L. Su, X. Liu, W. Gao, T. Wang, Y. Ma, Y. Zhong, X.-B. Cheng, Z. Zhu, J. He, Y. Wu, An examination and prospect of stabilizing li metal anode in lithium–sulfur batteries: a review of latest progress, Electron 1 (2) (2023) e13, https://doi.org/10.1002/elt2.13.
[3] Q. Liu, Z. Zheng, P. Xiong, C. Huang, S. Huang, B. Zhao, Y. Wu, Y. Zhang, B.-K. Kim, X. Yu, H.S. Park, Functional organic 7,7,8,8-tetracyanoquinodimethane artificial layers for the dendrite suppressed lithium metal anodes, Electron 2 (4) (2024) e72, https://doi.org/10.1002/elt2.72.
[4] B. Tong, X. Li, Towards separator safety of lithium-ion batteries: a review, Mater. Chem. Front. 8 (2) (2024) 309–340, https://doi.org/10.1039/D3QM00951C.
[5] C.J. Orendorff, T.N. Lambert, C.A. Chavez, M. Bencomo, K.R. Fenton, Polyester separators for lithium-ion cells: improving thermal stability and abuse tolerance, Adv. Energy Mater. 3 (3) (2013) 314–320, https://doi.org/10.1002/aenm.201200292.
[6] K.L. Jungjohann, R.N. Gannon, S. Goriparti, S.J. Randolph, L.C. Merrill, D. C. Johnson, K.R. Zavadil, S.J. Harris, K.L. Harrison, Cryogenic laser ablation reveals short-circuit mechanism in lithium metal batteries, ACS Energy Lett. 6 (6) (2021) 2138–2144, https://doi.org/10.1021/acsenergylett.1c00509.
[7] A.A. Heidari, H. Mahdavi, Recent development of polyolefin-based microporous separators for li−ion batteries: a review, Chem. Rec. 20 (6) (2020) 570–595, https://doi.org/10.1002/tcr.201900054.
[8] D. Chen, Y. Liu, C. Feng, Y. He, S. Zhou, B. Yuan, Y. Dong, H. Xie, G. Zeng, J. Han, W. He, Unified throughout-pore microstructure enables ultrahigh separator porosity for robust high-flux lithium batteries, Electron 1 (1) (2023) e1, https://doi.org/10.1002/elt2.1.
[9] Y. Ji, L. Dong, J. Liu, H. Xie, S. Zhong, C. Yang, J. Han, W. He, A li+-Flux-Homogenizing separator for long-term cycling of li metal anodes, Energy Environ. Sci. 17 (12) (2024) 4078–4089, https://doi.org/10.1039/D4EE00115J.
[10] W. Lu, Z. Yuan, Y. Zhao, H. Zhang, H. Zhang, X. Li, Porous membranes in secondary battery technologies, Chem. Soc. Rev. 46 (8) (2017) 2199–2236, https://doi.org/10.1039/C6CS00823B.
[11] C.F.J. Francis, I.L. Kyratzis, A.S. Best, Lithium-ion battery separators for ionic-liquid electrolytes: a review, Adv. Mater. 32 (18) (2020) 1904205, https://doi.org/10.1002/adma.201904205.
[12] A.L. Mong, Q.X. Shi, H. Jeon, Y.S. Ye, X.L. Xie, D. Kim, Tough and flexible, super ion-conductive electrolyte membranes for lithium-based secondary battery applications, Adv. Funct. Mater. 31 (12) (2021) 2008586, https://doi.org/10.1002/adfm.202008586.
[13] A. Kim, S.H. Oh, A. Adhikari, B.R. Sathe, S. Kumar, R. Patel, Recent advances in modified commercial separators for lithium–sulfur batteries, J. Mater. Chem. A 11 (15) (2023) 7833–7866, https://doi.org/10.1039/D2TA09266B.
[14] M.D. Hager, B. Esser, X. Feng, W. Schuhmann, P. Theato, U.S. Schubert, Polymer-based batteries—flexible and thin energy storage systems, Adv. Mater. 32 (39) (2020) 2000587, https://doi.org/10.1002/adma.202000587.
[15] X. Zhang, Q. Sun, C. Zhen, Y. Niu, Y. Han, G. Zeng, D. Chen, C. Feng, N. Chen, W. Lv, W. He, Recent progress in flame-retardant separators for safe lithium-ion batteries, Energy Storage Mater. 37 (2021) 628–647, https://doi.org/10.1016/j.ensm.2021.02.042.
[16] D. Lin, D. Zhuo, Y. Liu, Y. Cui, All-integrated bifunctional separator for li dendrite detection via novel solution synthesis of a thermostable polyimide separator, J. Am. Chem. Soc. 138 (34) (2016) 11044–11050, https://doi.org/10.1021/jacs.6b06324.
[17] Y. Yan, X. Liu, J. Yan, C. Guan, J. Wang, Electrospun nanofibers for new generation flexible energy storage, ENERGY & ENVIRONMENTAL MATERIALS 4 (4) (2021) 502–521, https://doi.org/10.1002/eem2.12146.
[18] F. Wang, X. Ke, K. Shen, L. Zhu, C. Yuan, A critical review on materials and fabrications of thermally stable separators for lithium-ion batteries, Advanced Materials Technologies 7 (5) (2022) 2100772, https://doi.org/10.1002/admt.202100772.
[19] B. Zheng, X. Lin, X. Zhang, D. Wu, K. Matyjaszewski, Emerging functional porous polymeric and carbonaceous materials for environmental treatment and energy storage, Adv. Funct. Mater. 30 (41) (2020) 1907006, https://doi.org/10.1002/adfm.201907006.
[20] X. Dai, X. Zhang, J. Wen, C. Wang, X. Ma, Y. Yang, G. Huang, H.-M. Ye, S. Xu, Research progress on high-temperature resistant polymer separators for lithium-ion batteries, Energy Storage Mater. 51 (2022) 638–659, https://doi.org/10.1016/j.ensm.2022.07.011.
[21] D. Li, H. Zhang, X. Li, Porous polyetherimide membranes with tunable morphology for lithium-ion battery, J. Membr. Sci. 565 (2018) 42–49, https://doi.org/10.1016/j.memsci.2018.08.011.
[22] J.-Y. Shi, Z. Liu, H. Yu, Y.-J. Li, Predicting drug-target interactions via within-score and between-score, BioMed Res. Int. (1) (2015) 350983, https://doi.org/10.1155/2015/350983, 2015.
[23] D. Li, D. Shi, Y. Xia, L. Qiao, X. Li, H. Zhang, Superior thermally stable and nonflammable porous polybenzimidazole membrane with high wettability for high-power lithium-ion batteries, ACS Appl. Mater. Interfaces 9 (10) (2017) 8742–8750, https://doi.org/10.1021/acsami.6b16316.
[24] Y. Meng, X. Du, Y. Xie, Z. li, S. Wang, Z. Liang, L. Cheng, X. Li, Nonsolvent-induced phase separation pPAN separators for dendrite-free rechargeable aluminum

batteries, ACS Appl. Mater. Interfaces (2024), https://doi.org/10.1021/acsami.4c03746.
[25] M. Li, Z. Zhang, Y. Yin, W. Guo, Y. Bai, F. Zhang, B. Zhao, F. Shen, X. Han, Novel polyimide separator prepared with two porogens for safe lithium-ion batteries, ACS Appl. Mater. Interfaces 12 (3) (2020) 3610–3616, https://doi.org/10.1021/acsami.9b19049.
[26] O. Lebedeva, D. Kultin, L. Kustov, Polymeric ionic liquids: here, there and everywhere, Eur. Polym. J. 203 (2024) 112657, https://doi.org/10.1016/j.eurpolymj.2023.112657.
[27] Y.S. Ye, J. Rick, B.J. Hwang, Ionic liquid polymer electrolytes, J. Mater. Chem. A 1 (8) (2013) 2719–2743, https://doi.org/10.1039/c2ta00126h.
[28] R.C. McNulty, E. Hampson, L.N. Cutler, C.P. Grey, W.M. Dose, L.R. Johnson, Understanding the limits of Li-NMC811 half-cells, J. Mater. Chem. A 11 (34) (2023) 18302–18312, https://doi.org/10.1039/D3TA00912B.
[29] P.G. Bruce, J. Evans, C.A. Vincent, Conductivity and transference number measurements on polymer electrolytes, Solid State Ionics 28–30 (1988) 918–922, https://doi.org/10.1016/0167-2738(88)90304-9.
[30] S. Buechele, E. Logan, T. Boulanger, S. Azam, A. Eldesoky, W. Song, M.B. Johnson, M. Metzger, Reversible self-discharge of LFP/graphite and NMC811/Graphite cells originating from redox shuttle generation, J. Electrochem. Soc. 170 (1) (2023) 010518, https://doi.org/10.1149/1945-7111/acb10c.
[31] Y.-C. Chien, H. Liu, A.S. Menon, W.R. Brant, D. Brandell, M.J. Lacey, Rapid determination of solid-state diffusion coefficients in Li-based batteries via intermittent current interruption method, Nat. Commun. 14 (1) (2023) 2289, https://doi.org/10.1038/s41467-023-37989-6.
[32] X. Yang, S.R. Liew, R. Bai, Simultaneous alkaline hydrolysis and non-solvent induced phase separation method for polyacrylonitrile (PAN) membrane with highly hydrophilic and enhanced anti-fouling performance, J. Membr. Sci. 635 (2021) 119499, https://doi.org/10.1016/j.memsci.2021.119499.
[33] J.U. Garcia, T. Iwama, E.Y. Chan, D.R. Tree, K.T. Delaney, G.H. Fredrickson, Mechanisms of asymmetric membrane formation in nonsolvent-induced phase separation, ACS Macro Lett. 9 (11) (2020) 1617–1624, https://doi.org/10.1021/acsmacrolett.0c00609.
[34] M. Waqas, S. Ali, C. Feng, D. Chen, J. Han, W. He, Recent development in separators for high-temperature lithium-ion batteries, Small 15 (33) (2019) 1901689, https://doi.org/10.1002/smll.201901689.
[35] A.K. Thakur, A. Kumar, H. Park, H. Kim, M.S. Ahmed, A.M. Saleque, M.P. Vikram, R. Saidur, Y. Ma, J.-Y. Hwang, Composite separators for internal thermal management in rechargeable lithium batteries: a review, J. Energy Storage 73 (2023) 108873, https://doi.org/10.1016/j.est.2023.108873.
[36] D.M.D. Babiker, Z.R. Usha, C. Wan, M.M.E. Hassaan, X. Chen, L. Li, Recent progress of composite polyethylene separators for lithium/sodium batteries, J. Power Sources 564 (2023) 232853, https://doi.org/10.1016/j.jpowsour.2023.232853.
[37] M. Wang, X. Chen, H. Wang, H. Wu, X. Jin, C. Huang, Improved performances of lithium-ion batteries with a separator based on inorganic fibers, J. Mater. Chem. A 5 (1) (2017) 311–318, https://doi.org/10.1039/C6TA08404D.
[38] B.J. Park, J.-S. Yu, K. Shin, Y. Kim, Polysiloxane-coated PI nonwoven separators with higher thermal and electrochemical stability for lithium ion battery application, Next Energy 3 (2024) 100090, https://doi.org/10.1016/j.nxener.2023.100090.
[39] S. Yao, Y. Yang, Z. Liang, J. Chen, J. Ding, F. Li, J. Liu, L. Xi, M. Zhu, J. Liu, A dual−Functional cationic covalent organic frameworks modified separator for high energy lithium metal batteries, Adv. Funct. Mater. 33 (13) (2023) 2212466, https://doi.org/10.1002/adfm.202212466.
[40] Y.S. Ye, M.G. Mohamed, M.C. Tsai, H.Y. Hu, B.J. Hwang, S.W. Kuo, Crown ether functionalized large-area graphene oxide and MXene hybridize as ion-sieving layers for high-performance lithium-sulfur batteries, J. Mater. Chem. A 12 (37) (2024) 25346–25358, https://doi.org/10.1039/d4ta04005h.
[41] Y.S. Ye, M.G. Mohamed, W.C. Chen, S.W. Kuo, Integrating the multiple functionalities in metalloporphyrin porous organic polymers enabling strong polysulfide anchoring and rapid electrochemical kinetics in Li-S batteries, J. Mater. Chem. A 11 (16) (2023) 9112–9124, https://doi.org/10.1039/d2ta09232h.
[42] J. Kim, S. Park, S. Hwang, W.-S. Yoon, Principles and applications of galvanostatic intermittent titration technique for lithium-ion batteries, J. Electrochem. Sci. Technol 13 (1) (2022) 19–31, https://doi.org/10.33961/jecst.2021.00836.